Available online at www.sciencedirect.com
ScienceDirect
Trans. Nonferrous Met. Soc. China 35(2025) 1704−1712
Transactions of Nonferrous Metals Society of China
www.tnmsc.cn

Electrochemical evaluation of Fe^{2+} ions in $MgCl_2$−NaCl−KCl melt

Jia ZHAO[1,2], Zhao-ting LIU[1,2] , Gui-min LU[1,2]

1. National Engineering Research Center for Integrated Utilization of Salt Lake Resource, East China University of Science and Technology, Shanghai 200237, China;
2. Joint International Laboratory for Potassium and Lithium Strategic Resources, East China University of Science and Technology, Shanghai 200237, China

Received 30 September 2023; accepted 27 May 2024

Abstract: A comprehensive electrochemical assessment of Fe^{2+} behavior in a $MgCl_2$−NaCl−KCl melt was reported, involving cyclic voltammetry (CV), square wave voltammetry (SWV), and chronoamperometry (CA) analyses. Reduction of Fe^{2+} in $MgCl_2$−NaCl−KCl was observed to occur in a single step involving two electrons, exhibiting quasi-reversible behavior. The diffusion coefficient of Fe^{2+} (5.75×10^{-5} cm^2/s) in this system was experimentally determined at 973 K, with an associated diffusion activation energy of 25.06 kJ/mol in the range of 973−1048 K, and an estimated standard rate constant for Fe^{2+}/Fe of around 1×10^{-3} cm/s. The nucleation of Fe on the tungsten electrode in the $MgCl_2$−NaCl−KCl molten salt is insensitive to temperature and overpotential. It is found that the nucleation mode is related to the concentration of Fe^{2+} surrounding the electrode and evolves from an instantaneous to a progressive process, accompanied by a deterioration of magnesium electrolysis due to Fe impurities.
Key words: Fe^{2+}; $MgCl_2$−NaCl−KCl melt; electrochemical reduction; kinetic properties; nucleation mechanism

1 Introduction

Magnesium (Mg) is one of the lightest metallic structural materials, and its alloys are considered the “green engineering material of the twenty-first century”. These alloys find widespread use across diverse sectors, including aerospace [1], 3C products [2], biomedical [3,4], and automotive industries [5,6], due to their low density, superior damping performance, and recyclability [7]. As the utilization of magnesium continues to expand, attention has increasingly turned to effective production methods. In this context, molten salt electrolysis has emerged as a prominent alternative to the traditional Pidgeon process [8], owing to its high production efficiency, resource utilization, low energy consumption, and low environmental impact [9−11]. Consequently, optimization of the molten salt electrolysis process is a priority requirement to enable the sustainable development of the magnesium industry.

Iron (Fe) is regarded as the most hazardous impurity in magnesium electrolytes, influencing current efficiency in magnesium electrolysis processes. When the Fe content is maintained at 0.01%, the current efficiency ranges from 88% to 90%, decreasing to 69.3% in the presence of 0.3% Fe. The Fe^{2+} component can undergo reduction at the cathode to generate an iron sponge that subsequently adsorbs MgO and passivates the cathode surface. In addition, the $FeCl_2$-containing electrolyte can wet the iron cathode, resulting in magnesium precipitation in the form of caviar-like clusters that are prone to loss. The iron that is generated can adsorb on the surface of magnesium

Corresponding author: Gui-min LU, Tel: +86-21-64252173, E-mail: gmlu@ecust.edu.cn
https://doi.org/10.1016/S1003-6326(25)66777-X

beads, causing an increase in bead mass and subsequent incorporation into the slag phase.

There are a number of reported studies of Fe ions in molten salts. INMAN et al [12] claimed that the electrochemical reduction of Fe^{2+} can be represented by $Fe^{2+}+2e=Fe$, which was identified as a diffusion-controlled process in the LiCl−KCl system. NEWTON et al [13] evaluated the activity coefficient of $FeCl_2$ in LiCl−KCl−$FeCl_2$, which ranged from 2.95×10^{-5} to 1.01×10^{-4}, and was unaffected by low concentrations of NaCl, $LaCl_3$, and CsCl. YOON and CHOI [14] investigated the diffusion coefficient and standard rate constant of Fe^{2+} in the melt at 773 K based on cyclic voltammetry and numerical fitting. The reported diffusion coefficients were about 1×10^{-5} cm^2/s with a standard rate constant of around 1×10^{-3} cm/s. KHALAGHI et al [15] conducted an electrochemical analysis of iron in the LiCl−KCl−NaCl system at 823 K, and noted that Fe^{2+}/Fe conversion was coupled with a chemical reaction. Moreover, the Fe^{2+} diffusion coefficient in the melt was determined to be 1.4×10^{-5} cm^2/s. LUGOVSKOY et al [16] has explored the electroreduction of Fe^{2+} on platinum electrodes in NaCl−KCl, where Fe deposition was found to be an irreversible process with charge transfer leading to Fe−Pt alloy formation as rate-determining. GE et al [17] considered the electrochemical behavior of Fe^{3+} on glassy carbon electrodes without a Fe^{3+}/Fe^{2+} contribution, and attributed the low diffusion coefficient of Fe^{3+} to an evaporation of $FeCl_3$ that lowered the concentration of Fe^{3+} in the melt. In the case of $ZnCl_2$−NaCl at 723 K, LEE et al [8] established the stability of both Fe^{2+} and Fe^{3+} in the melt. They noted that the reduction processes involving Fe^{3+}/Fe^{2+} and Fe^{2+}/Fe were quasi-reversible and diffusion-controlled. In addition, they observed an instantaneous deposition of Fe on glassy carbon electrodes. NIAZI et al [18] investigated the electrodeposition of $FeCl_2$ and $FeCl_3$, where Fe removal was conducted using a zinc electrode in a $ZnCl_2$−KCl−NaCl melt. In the case of the $MgCl_2$−NaCl−KCl system, WANG et al [19] claimed that Fe^{3+} remained stable at 973 K in the molten salt. They confirmed that Fe^{3+} reduction proceeded in a diffusion-controlled quasi-reversible single step involving three electrons, and demonstrated a progressive Fe deposition.

Despite the extensive research on Fe electrochemical processes in molten states, the behavior of Fe^{2+} in magnesium electrolysis systems is not fully understood. This study represents the first attempt to comprehensively evaluate the electrochemical characteristics of Fe^{2+} in $MgCl_2$−NaCl−KCl, using a range of electrochemical techniques. The electroreduction mechanism of Fe^{2+} was explained, and a comprehensive kinetic database was established. In addition, we have considered the mechanism of Fe nucleation on the electrode substrate, and the associated effect on magnesium electrolysis. The findings of this study provide a better understanding of the electro-reduction dynamics of Fe impurities during magnesium electrolysis, and can contribute to advance in the magnesium electrolysis industry.

2 Experimental

NaCl (>99.0%, Aladdin), KCl (>99.0%, Aladdin), and $FeCl_2$ (>99.0%, Aladdin) were supplied by Shanghai Aladdin Biochemical Technology Co., Ltd., and $MgCl_2$ (>99.0%, Macklin) was obtained from Shanghai Zhonghe Chemical Technology Co., Ltd. All the reagents underwent vacuum drying at 473 K for 24 h, and were then stored in a glove box (Mikrouna). For each experiment, 100 g $MgCl_2$−NaCl−KCl-mixed salt (mass ratio=10∶45∶45) was placed in a graphite crucible in the glove box, then transferred to a resistance furnace and heated to the desired temperature. The potentiostatic method at −1.21 V (vs Ag/AgCl) was applied for 2.5 h as a pre-electrolysis step to purify the melts, removing metal ions. Subsequently, $FeCl_2$ was introduced into the system as a source of Fe^{2+}, accompanied by 0.5 h of argon bubbling to ensure system homogeneity. A continuous supply of argon gas throughout the experiment maintained an inert atmosphere, avoiding the effects of water and oxygen. Following each electrochemical test, the working electrode underwent cleaning by applying an anodic current for 90 s, followed by a pause of 120 s to allow the system to equilibrate.

All the electrochemical measurements were carried out using the Princeton 4000 electro-chemical workstation, controlled by the Versa-Studio software package. The electrochemical experiments were conducted in a three-electrode system with a tungsten rod serving as the working electrode, polished using various grades of sandpaper. A spectral pure graphite rod was utilized

as an auxiliary electrode, and an in-house fabricated Ag/AgCl in the NaCl−KCl−$MgCl_2$−AgCl mixture was employed as a reference electrode. All the potentials were referenced to Ag/AgCl electrodes. The active area of the working electrode was adjusted using an in-house micro-positioning apparatus to control its depth. The melt temperature was monitored during experiments using thermocouples inserted in corundum tubes, with an accuracy of ±1 K.

3 Results and discussion

3.1 Electrochemical reduction mechanism of Fe^{2+}

3.1.1 Cyclic voltammetry (CV) analysis

The CV curves obtained using a tungsten electrode in $MgCl_2$−NaCl−KCl melts, before and after the addition of $FeCl_2$ at 973 K are presented in Fig. 1. The black profile illustrates a typical CV response for the $MgCl_2$−NaCl−KCl salt. Peak B, observed at −1.32 V, corresponds to the deposition of Mg, whereas the anodic peak B′ at −1.24 V indicates Mg dissolution during the reverse scan direction. The addition of 1 wt.% $FeCl_2$ (red profile) results in a new redox pair A/A′ alongside B/B' in the CV curve, with a reduction peak potential of −0.12 V and an oxidation peak potential at 0.17 V. The A/A′ pair corresponds to the formation and dissolution of metallic iron.

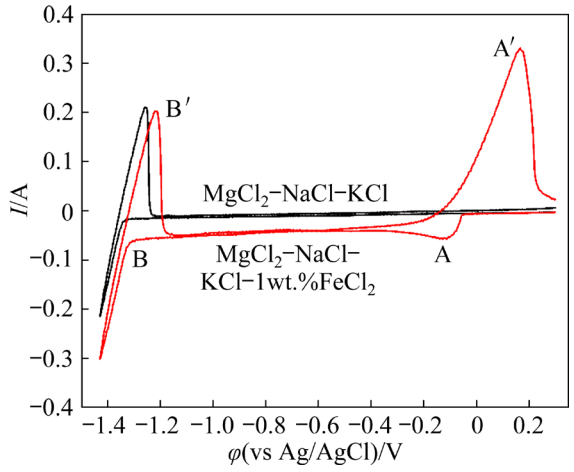

Fig. 1 CV analysis of $MgCl_2$−NaCl−KCl and $MgCl_2$−NaCl−KCl−1wt.%$FeCl_2$ at 973 K, scanning rate=0.1 V/s, and electrode area A=0.3535 cm^2

3.1.2 Square-wave voltammetry (SWV) analysis

The use of SWV enables an accurate determination of the number of electron transfer in electrochemical reactions. The relationship between the peak width at half maximum height obtained from SWV, electron transfer number, and temperature is expressed as

$$W_{1/2} = 3.5RT/(nF) \quad (1)$$

where $W_{1/2}$ represents the peak width at half maximum height, R denotes the molar gas constant, T is the temperature, n represents the number of electrons exchanged, and F is the Faraday constant.

The current associated with $MgCl_2$−NaCl−KCl−1wt.%$FeCl_2$ as a function of potential is illustrated in Fig. 2 for SWV measurement from 0.3 to −1.45 V. The asymmetric peak observed at around 0 V corresponds to the reduction of Fe^{2+}, consistent with the CV results. It should be noted that the asymmetric peak is attributed to the overpotential of the Fe^{2+} electrochemical reduction, which causes a delay occurring in the current increase during reduction, resulting in a steeper current increase relative to decay.

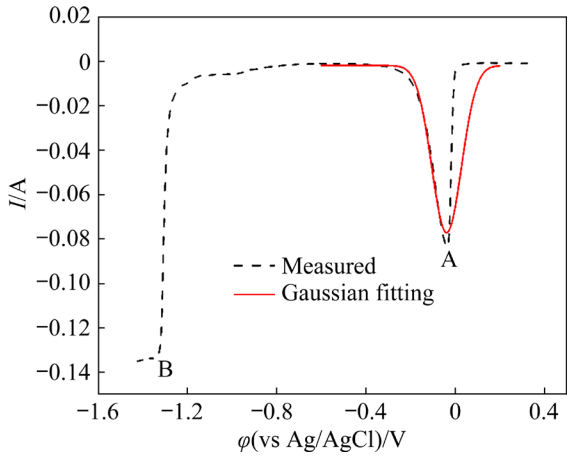

Fig. 2 SWV results of $MgCl_2$−NaCl−KCl−1wt.%$FeCl_2$ using tungsten electrode (A=0.3535 cm^2) at 973 K

In order to determine the $W_{1/2}$ of the reduction peak, the current decrease peak component was employed for Gaussian fitting (red curve) [20], resulting in $W_{1/2}$=0.13 V. This corresponds to a calculated transfer of 2.26 electrons, which confirms the reduction of Fe^{2+} to metallic Fe in $MgCl_2$−NaCl−KCl occurring in one step with two electrons. This result suggests that Fe^{2+} is directly electrodeposited on the tungsten electrode as follows:

$$Fe^{2+}+2e=Fe \quad (2)$$

3.1.3 Reversibility analysis

The reversibility of Fe^{2+} reduction was assessed by successive CV analyses, from 0.1 to 0.5 V/s. The variation of current with potential at different scanning rates is shown in Fig. 3. It can be seen that $\Delta\varphi_p$ ($|\varphi_{pa}-\varphi_{pc}|$, the difference between the peak potential for oxidation and reduction), which is independent of scanning rate in a reversible process, increased with increasing scanning rate, accompanied by a successive increase in the peak current for the reduction/oxidation of Fe. This response suggests that Fe^{2+} reduction in the $MgCl_2$−NaCl−KCl melt is not reversible.

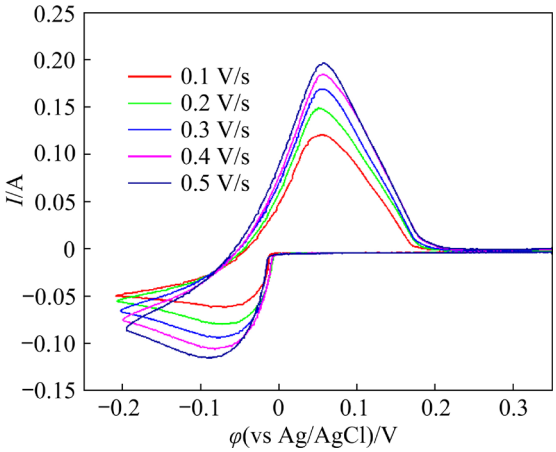

Fig. 3 CV results of Fe^{2+} reduction on tungsten electrode (A=0.3535 cm^2) and subsequent oxidation at different scanning rates

The relationship between the square root of scanning rate ($v^{1/2}$) and the cathode peak current (I) obtained from Fig. 3 is presented in Fig. 4. A linear dependence of I on $v^{1/2}$, passing through the origin, suggests that the reduction is a reversible or irreversible process. When the dependency deviates from linear, the process is regarded as quasi-reversible [21]. As shown in Fig. 4, the relationship gradually deviates from linear at higher scanning rates, suggesting that Fe^{2+} reduction in $MgCl_2$−NaCl−KCl melt belongs to the quasi-reversible category.

The reversibility of Fe^{2+} reduction was assessed semi-quantitatively, using the diagnostic parameter Λ, expressed as

$$\Lambda=\frac{k^0}{[DnF/(RT)]^{1/2}}\frac{1}{v^{1/2}} \quad (3)$$

where k^0 and D represent the standard rate constant and diffusion coefficient, respectively. The reversibility of a reaction can be determined based on Λ. When $\Lambda\geq15$, the reaction is considered reversible; when $\Lambda\leq10^{-2(1+\alpha)}$, it falls into the irreversible category, and all other cases are classified as quasi-reversible [22]. The parameter α is defined as the transfer coefficient, and a value of 0.5 was applied in this work [23,24]. The deposition of Fe^{2+} in $MgCl_2$−NaCl−KCl at 973 K resulted in Λ values of 0.094 and 0.166 at 0.5 V/s and 0.1 V/s, respectively. Therefore, the Fe^{2+}/Fe reaction can be considered quasi-reversible.

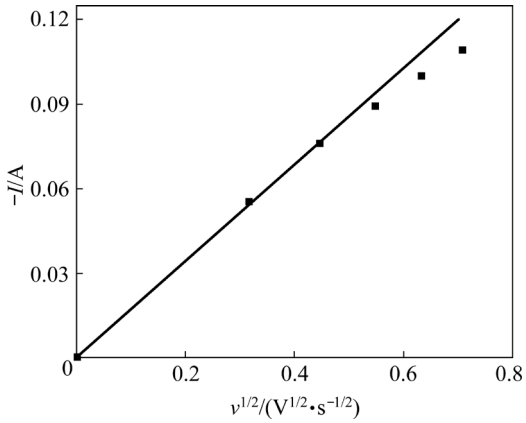

Fig. 4 Relationship between current and square root of scanning rate (A=0.3535 cm^2)

3.2 Kinetic properties

3.2.1 Diffusion coefficient

In order to evaluate the kinetic properties of Fe^{2+} reduction, the CV curve (v=0.5 V/s) in Fig. 3 was subjected to semi-integral analysis [25,26], and the resultant convolution curve is shown in Fig. 5.

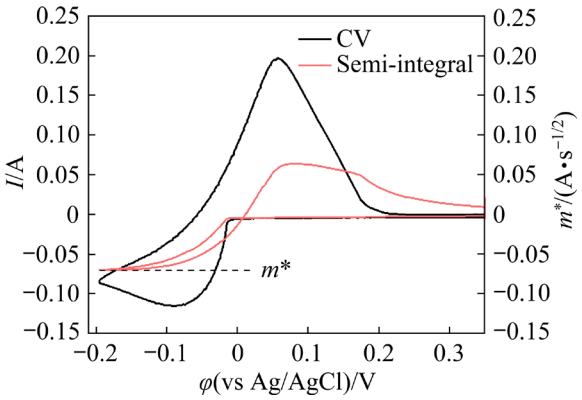

Fig. 5 CV results at 0.5 V/s and corresponding semi-integral curve at 973 K (A=0.3535 cm^2)

It is clear that the semi-integrated curves do not agree with the forward and reverse scanning currents, and present limits at the high cathodic

potential range, suggesting that Fe^{2+} reduction is diffusion-controlled. When Fe^{2+} near the electrode surface becomes depleted, the curve reaches the semi-integrated current limit m^*, which is applied to assessing the ionic diffusion coefficient using Eq. (4):

$$m^* = -nFAC_0\sqrt{D} \tag{4}$$

where A represents the electrode area, and C_0 is the bulk concentration of Fe^{2+} in the melt. The calculated Fe^{2+} diffusion coefficient at 973 K is 5.75×10^{-5} cm^2/s. The diffusion coefficients at other temperatures derived using the semi-integral method are given in Table 1.

Table 1 Fe^{2+} diffusion coefficients in $MgCl_2$−NaCl−KCl molten salt at 973−1048 K obtained from semi-integral analysis

Temperature/K	D/(10^{-5} cm^2·s^{-1})
973	5.75
998	6.18
1023	6.65
1048	7.18

The linear relationship between the logarithm of the diffusion coefficient and temperature is presented in Fig. 6, and is expressed as

$$\ln D = -6.67 - 25064.22/(RT) \tag{5}$$

The associated Fe^{2+} diffusion activation energy derived from the slope is 25.06 kJ/mol. These findings serve as valuable reference data for guiding the separation and extraction of Fe from magnesium electrolysis systems, and optimizing the design of electrolytic cells for industrial application.

3.2.2 Standard rate constant

The standard rate constant for the Fe^{2+}/Fe reaction in the melt was assessed using the Nicholson method. Initially, a working plot of $n\Delta\varphi_p$ versus $\lg\psi$ was constructed from data reported in the literature [27,28], which is presented in Fig. 7. The CV curves at scanning rates of 0.5 and 0.1 V/s (Fig. 3) were used to determine the corresponding ψ values by combining the working curves.

The standard rate constants (k^0) for the Fe^{2+}/Fe reaction at different scanning rates were determined using Eq. (6), yielding values of 2.47×10^{-3} and 1.94×10^{-3} cm/s at 0.5 and 0.1 V/s, respectively. The detailed calculations are demonstrated in Fig. 7.

$$\psi = \frac{k^0}{[DnF\pi/(RT)]^{1/2}}\frac{1}{v^{1/2}} \tag{6}$$

where ψ is the parameter associated with D and k^0.

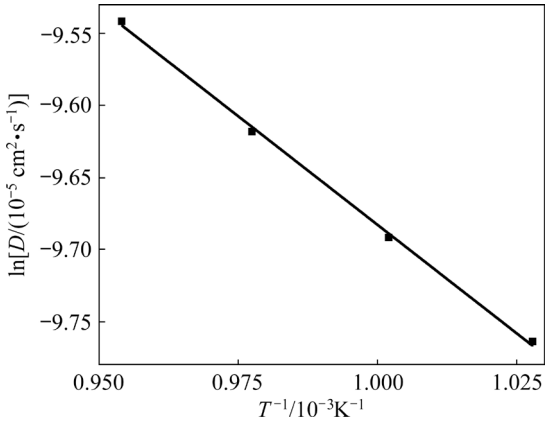

Fig. 6 Correlation of $\ln D$ with $1/T$ for $MgCl_2$−NaCl−KCl melt at 973−1048 K

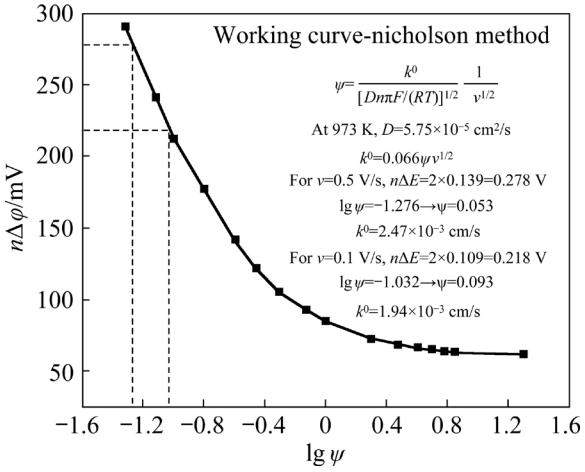

Fig. 7 Working curve based on Nicholson method for determining standard rate constant

3.3 Nucleation mechanism

In molten salts, chronoamperometry (CA) analysis was extensively utilized to investigate the nucleation mechanism of metal ions on electrode substrates. The technique records the temporal variation of current under a constant potential pulse. The change in current (I) over time (t) on the tungsten electrode in the $MgCl_2$−NaCl−KCl−$FeCl_2$ system is shown in Fig. 8 at different applied potentials. The entire CA response can be categorized into three periods. Initially, the current rises rapidly to reach a peak, corresponding to the nucleation and subsequent growth of Fe with an expansion of the active area. Subsequently, the current gradually decreases, influenced by the

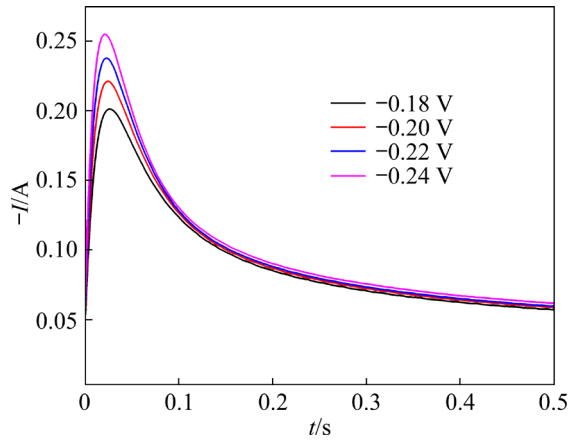

Fig. 8 *I*–*t* transient curves for $MgCl_2$–NaCl–KCl–1wt.%$FeCl_2$ at 973 K with varying potentials (A=0.3535 cm^2)

diffusion of Fe^{2+} in the system. Finally, the current stabilizes as the mass transfer and reduction reactions reach equilibrium. It is evident that the system responds with large currents when the potential is negatively shifted, suggesting that the applied potential can supply sufficient overpotential for Fe nucleation.

We employed two non-dimensional models, proposed by GUNAWARDENA et al [29] and SCHARIFKER and HILLS [29,30], to determine the Fe nucleation pattern on the electrode substrate by analyzing the CA results. The associated detailed expressions are presented in Eqs. (7) and (8):

In the case of instantaneous nucleation:

$$\left(\frac{I}{I_m}\right)^2=1.9542\left(\frac{t_m}{t}\right)\left\{1-\exp\left[-1.2564\left(\frac{t}{t_m}\right)\right]\right\}^2 \quad (7)$$

In the case of progressive nucleation:

$$\left(\frac{I}{I_m}\right)^2=1.2254\left(\frac{t_m}{t}\right)\left\{1-\exp\left[-2.3367\left(\frac{t}{t_m}\right)^2\right]\right\}^2 \quad (8)$$

where I_m is peak current, t denotes time, and t_m is the time corresponding to the peak current.

A comparison of the experimental data obtained from $MgCl_2$–NaCl–KCl–1wt.%$FeCl_2$ melts at different temperatures in terms of the instantaneous and progressive nucleation models is presented in Fig. 9, covering potentials from −0.18 to −0.24 V. At each temperature, the mode of

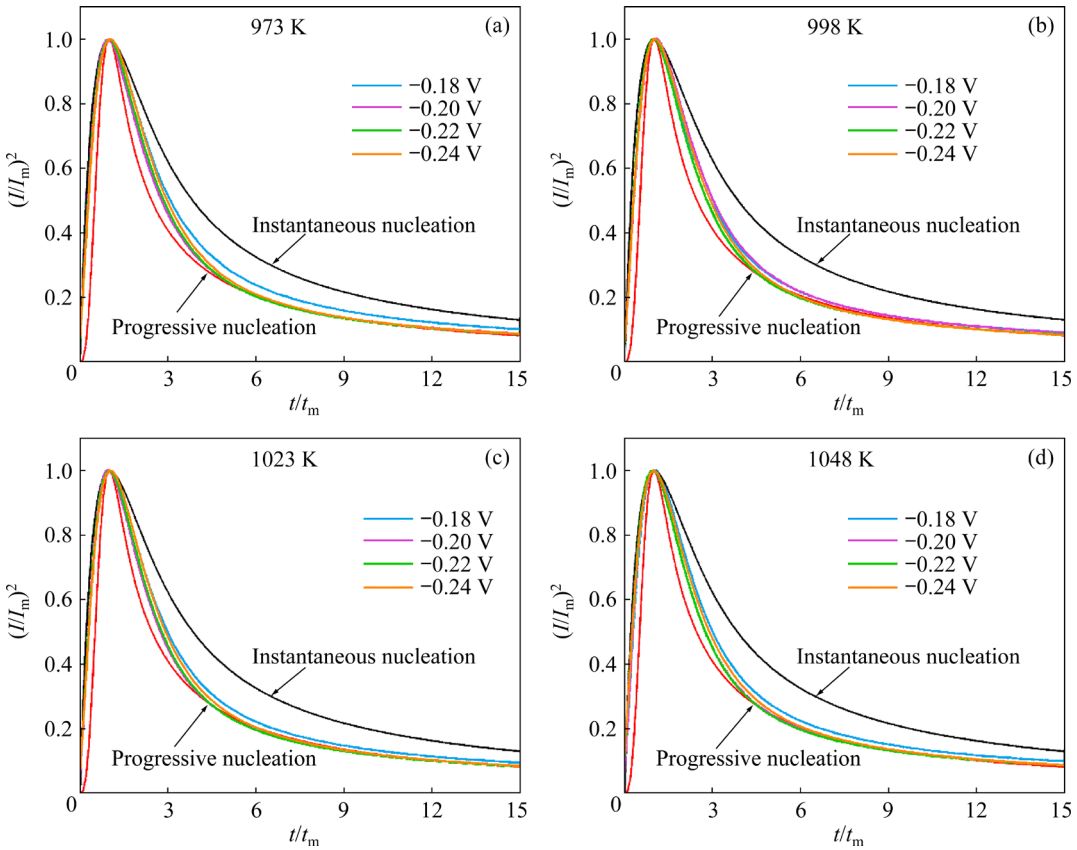

Fig. 9 Comparison of Fe nucleation mode on electrode in terms of theoretical non-dimensional nucleation models in $MgCl_2$–NaCl–KCl–1wt.%$FeCl_2$ system at different temperatures and potentials

nucleation corresponding to each potential follows a consistent pattern. When $t < t_m$, nucleation occurs instantaneously; as time progresses, nucleation shifts from instantaneous to progressive, ultimately reaching progressive nucleation at extended time. In analyzing the evolution of nucleation with the I–t curve presented in Fig. 8, it is evident that the stage of rapid current increase corresponds to an instantaneous nucleation of Fe on the electrode, facilitated by an ample supply of Fe^{2+} ions near the electrode. As the Fe^{2+} becomes depleted and the process is diffusion-controlled, the nucleation transitions from instantaneous to progressive and eventually stabilizes as the progressive mode. The results indicate that the mode of Fe nucleation on the electrode in the $MgCl_2$−NaCl−KCl−1wt.%$FeCl_2$ melt is dependent on the Fe^{2+} concentration surrounding the electrode. There is no significant variance in the nucleation pattern from 973 to 1048 K across all applied potentials, suggesting that the experimental tests have a sufficiently supplied overpotential.

In progressive nucleation, the increased formation of nuclei is accompanied by the generation of new nuclei, resulting in an uneven distribution. In contrast, nuclei are only generated at the initiation of deposition in instantaneous nucleation, followed by growth. In the $MgCl_2$−NaCl−KCl−1wt.%$FeCl_2$ molten salt system, Fe nucleation ultimately reaches a stable progressive mode that corresponds to the sponge-like iron deposition on the electrode during magnesium electrolysis. This observation is consistent with our previous report [31], suggesting that spongy iron serves to impede magnesium electrolysis, leading to a deposition of magnesium products that have the appearance of “caviar”. Consequently, magnesium electrolysis is negatively impacted by Fe impurities.

4 Conclusions

(1) The Fe^{2+} deposition on a tungsten electrode in the $MgCl_2$−NaCl−KCl melt proceeds through a one-step process, involving the transfer of two electrons. Furthermore, the quasi-reversible behavior of Fe^{2+} reduction was confirmed by CV measurements.

(2) The experimentally determined Fe^{2+} diffusion coefficient in this system at 973 K is 5.75×10^{-5} cm^2/s, using the semi-integral method. The associated diffusion activation energy (973−1048 K) is 25.06 kJ/mol, with a standard rate constant of around 1×10^{-3} cm/s.

(3) The progression of nucleation was investigated using the CA technique. In the $MgCl_2$−NaCl−KCl−1wt.%$FeCl_2$ melt, the Fe nucleation mechanism is insensitive to temperature and over-potential, and depends on the Fe^{2+} concentration around the electrode. The process evolved from instantaneous to progressive nucleation, where magnesium electrolysis was impeded by the presence of Fe impurities.

CRediT authorship contribution statement

Jia ZHAO: Conceptualization, Methodology, Formal analysis, Writing − Original draft; **Zhao-ting LIU:** Data curation, Visualization, Investigation; **Gui-min LU:** Funding acquisition, Resources, Supervision, Writing − Review & editing.

Declaration of competing interest

The authors declare that they have no known competing financial interests or personal relationships that could have appeared to influence the work reported in this paper.

Acknowledgments

The authors acknowledge the financial support provided by the National Key R&D Program of China (No. 2022YFB3709300).

References

[1] TAN J, RAMAKRISHNA S. Applications of magnesium and its alloys: A review [J]. Applied Sciences, 2021, 11(15): 6861.

[2] YANG Y, XIONG X M, CHEN J, PENG X D, CHEN D L, PAN F S. Research advances in magnesium and magnesium alloys worldwide in 2020 [J]. Journal of Magnesium and Alloys, 2021, 9(3): 705−747.

[3] LI N, ZHENG Y F. Novel magnesium alloys developed for biomedical application: A review [J]. Journal of Materials Science & Technology, 2013, 29(6): 489−502.

[4] XIN Y, HU T, CHU P K. In vitro studies of biomedical magnesium alloys in a simulated physiological environment: A review [J]. Acta Biomaterialia, 2011, 7(4): 1452−1459.

[5] WANG G G, WEILER J P. Recent developments in high-pressure die-cast magnesium alloys for automotive and future applications [J]. Journal of Magnesium and Alloys, 2023, 11(1): 78−87.

[6] BALAJI V, RAJA V K B, PALANIKUMAR K, PONSHANMUGAKUMAR, ADITYA N, ROHIT V. Effect of heat treatment on magnesium alloys used in automotive industry: A review [J]. Materials Today: Proceedings, 2021, 46: 3769−3771.

[7] MA Ya-jie, LIU Chu-ming, JIANG Shu-nong, GAO Yong-hao, WAN Ying-chun, CHEN Zhi-yong. Tailoring good combinations among strength, ductility and damping capacity in a novel Mg−1.5Gd−1Zn damping alloy via hot extrusion [J]. Materials Science and Engineering: A, 2023, 871: 144827.

[8] LEE T H, OKABE T H, LEE J Y, KIM Y M, KANG J. Development of a novel electrolytic process for producing high-purity magnesium metal from magnesium oxide using a liquid tin cathode [J]. Journal of Magnesium and Alloys, 2021, 9(5): 1644−1655.

[9] WU Xiao-bin, ZHU Zeng-li, KONG Hui, FAN You-qi, CHENG Si-wei, HUA Zhong-sheng. Electrochemical reduction mechanism of Zn^{2+} in molten NaCl−KCl eutectic [J]. Transactions of Nonferrous Metals Society of China, 2022, 32(9): 3088−3098.

[10] YUAN Rui, LÜ Cheng, WAN He-li, LI Shao-long, CHE Yu-si, HE Ji-lin, SONG Jian-xun. Effect of fluoride addition on electrochemical behaviors of V(III) in molten LiCl−KCl [J]. Transactions of Nonferrous Metals Society of China, 2022, 32(8): 2736−2745.

[11] ZHAO Jia, YAN Yi-hang, ZHANG Hao, GAO Hua-yang, ZHANG Ye, LU Gui-min. Electrochemical behavior of $MgCl_2$ and co-deposition mechanisms of Mg and Sr in $SrCl_2$−KCl−$MgCl_2$ melt [J]. Transactions of Nonferrous Metals Society of China, 2024, 34: 2381−2392.

[12] INMAN D, LEGEY J C, SPENCER R. A chrono-potentiometric study of iron in LiCl−KCl [J]. Journal of Applied Electrochemistry, 1978, 8: 269−272.

[13] NEWTON M, MERWIN A, MCMURRAY J, SIMPSON M. Effect of metal chloride impurities on equilibrium potential of Fe/$FeCl_2$ in eutectic LiCl−KCl [J]. Journal of the Electrochemical Society, 2023, 170(7): 076507.

[14] YOON S, CHOI S. Spectroelectrochemical behavior of Cr, Fe, Co, and Ni in LiCl−KCl molten salt for decontaminating radioactive metallic wastes [J]. Journal of the Electrochemical Society, 2021, 168(1): 013504.

[15] KHALAGHI B, KVALHEIM E, TOKUSHIGE M, TENG Li-dong, SEETHARAMAN S, HAARBERG G M. Electrochemical behaviour of dissolved iron chloride in KCl+LiCl+NaCl melt at 550 °C [J]. ECS Transactions, 2014, 64(4): 301−310.

[16] LUGOVSKOY A, ZINIGRAD M, AURBACH D, UNGER Z. Electrodeposition of iron(II) on platinum in chloride melts at 700−750 °C [J]. Electrochimica Acta, 2009, 54(6): 1904−1908.

[17] GE X L, XIAO S J, HAARBERG G M, SEETHARAMAN S. Salt extraction process-novel route for metal extraction Part 3-electrochemical behaviours of metal ions (Cr, Cu, Fe, Mg, Mn) in molten ($CaCl_2$) NaCl−KCl salt system [J]. Mineral Processing and Extractive Metallurgy, 2010, 119(3): 163−170.

[18] NIAZI S, OLSEN E, NYGÅRD H S. Electrochemical removal of Cu, Fe and Mn from molten $ZnCl_2$·KCl·NaCl [J]. Separation and Purification Technology, 2022, 299: 121705.

[19] WANG Y P, WANG J, ZENG Z, LIU H, HE S W, HUA Z S. Electrochemical separation of Fe(III) impurity from molten $MgCl_2$−NaCl−KCl for magnesium electrolytic production [J]. Separation and Purification Technology, 2023, 317: 123857.

[20] SU L L, LIU K, LIU Y L, WANG L, YUAN L Y, WANG L, LI Z J, ZHAO X L, CHAI Z F, SHI W Q. Electrochemical behaviors of Dy(III) and its co-reduction with Al(III) in molten LiCl−KCl salts [J]. Electrochimica Acta, 2014, 147: 87−95.

[21] TANG H, PESIC B. Electrochemical behavior of $LaCl_3$ and morphology of La deposit on molybdenum substrate in molten LiCl−KCl eutectic salt [J]. Electrochimica Acta, 2014, 119: 120−130.

[22] MATSUDA H, AYABE Y. On the theory of Randles-Sevčik cathode ray polarography [J]. Journal of Electrochemistry, Reports of the Bunsen Society for Physical Chemistry, 1955, 59(6): 494−503. (in German)

[23] SAHOO D K, SATPATI A K, KRISHNAMURTHY N. Electrochemical properties of Ce(III) in an equimolar mixture of LiCl−KCl and NaCl−KCl molten salts [J]. RSC Advances, 2015, 5(42): 33163−33170.

[24] LIU Z T, LU G M, YU J G. Investigation on electrochemical behaviors of Ni(II) impurity in LiCl−KCl melt [J]. Separation and Purification Technology, 2021, 268: 118354.

[25] GRENNESS M, OLDHAM K B. Semiintegral electroanalysis. Theory and verification [J]. Analytical Chemistry, 1972, 44(7): 1121−1129.

[26] GOTO M, OLDHAM K B. Semiintegral electroanalysis. Shapes of neopolarograms [J]. Analytical Chemistry, 1973, 45(12): 2043−2050.

[27] NICHOLSON R S. Theory and application of cyclic voltammetry for measurement of electrode reaction kinetics [J]. Analytical Chemistry, 1965, 37(11): 1351−1355.

[28] PERONE S P. Evaluation of stationary electrode polarography and cyclic voltammetry for the study of rapid electrode processes [J]. Analytical Chemistry, 1966, 38(9): 1158−1163.

[29] GUNAWARDENA G, HILLS G, MONTENEGRO I, SCHARIFKER B. Electrochemical nucleation: Part I. General considerations [J]. Journal of Electroanalytical Chemistry and Interfacial Electrochemistry, 1982, 138(2): 225−239.

[30] SCHARIFKER B, HILLS G. Theoretical and experimental studies of multiple nucleation [J]. Electrochimica Acta, 1983, 28(7): 879−889.

[31] LIU Z T, LU G M, YU J G. Effects of Fe (III) on $MgCl_2$ electrolysis and its cathodic processes on W electrodes [J]. Ionics, 2019, 25: 3945−3952.

$MgCl_2$−NaCl−KCl 熔体中的 Fe^{2+}离子的电化学评估

赵 佳[1,2]，刘兆庭[1,2]，路贵民[1,2]

1. 华东理工大学 国家盐湖资源综合利用工程技术研究中心，上海 200237；
2. 华东理工大学 钾锂战略资源国际联合实验室，上海 200237

摘 要：采用循环伏安、方波伏安和计时电流等电化学方法对 $MgCl_2$−NaCl−KCl 熔体中的 Fe^{2+}离子行为进行电化学评估。在 $MgCl_2$−NaCl−KCl 熔体中，Fe^{2+}的还原属于一步两电子的准可逆过程。在 973 K 下，Fe^{2+}在熔体中的扩散系数为 5.75×10^{-5} cm^2/s，且在 973~1048 K 温度范围内的扩散活化能为 25.06 kJ/mol。Fe^{2+}/Fe 的标准速率常数约为 1×10^{-3} cm/s。在 $MgCl_2$−NaCl−KCl 熔体中，钨电极表面上 Fe 的成核模式对温度和过电位不敏感，而与电极周围的 Fe^{2+}浓度有关，且成核模式均由瞬时成核演变为渐进成核，反映了 Fe 杂质恶化镁电解的机理。

关键词：Fe^{2+}；$MgCl_2$−NaCl−KCl 熔体；电化学还原；动力学性质；成核机理

(Edited by Xiang-qun LI)